Revista Mexicana de Astronomía y Astrofísica, **36**, 121–133 (2000)

HIGH RESOLUTION SPECTROSCOPIC STUDY OF ABELL 78 [1]

S. Medina and M. Peña

Instituto de Astronomía
Universidad Nacional Autónoma de México

Received 2000 June 9; accepted 2000 August 14

RESUMEN

Se analizan datos espectroscópicos de alta resolución de los nudos centrales y de la cáscara externa de la nebulosa planetaria Abell 78. Para cada región se deriva la composición química y se analiza la cinemática. Los nudos internos son más densos y ligeramente más fríos que la cáscara externa y su composición es muy deficiente en hidrógeno. Los nudos se están alejando de la estrella central con velocidades entre +40 y −60 km s^{-1} y muestran estructuras cometarias. La cáscara externa aparenta tener muy baja metalicidad y concluímos que la determinación de abundancias está posiblemente afectada por fluctuaciones de temperatura, debidas a mecanismos adicionales de calentamiento (choques y fotoelectrones emitidos por el polvo). El análisis cinemático demuestra que la emisión de H proviene de la cáscara externa. En la zona externa hemos encontrado una estructura compacta con velocidades entre −40 y 90 km s^{-1} que emite en líneas de excitación colisional (principalmente [O III]), pero no se detecta en H ni en He, por lo que debe tratarse de una "bala" de material deficiente en H, que está colisionando con la cáscara externa.

ABSTRACT

High resolution spectroscopic data of the central knots and the outer shell of the planetary nebula Abell 78 are analyzed. Chemical abundances and kinematics were derived for each region. The inner knots appear to be denser and slightly cooler than the outer shell, and they are constituted by an extremely H-deficient material. These knots are receding from the central star with velocities in the range from +40 to −60 km s^{-1} and present cometary structures probably caused by the stellar wind. The outer shell appears to have very low metallicity but we conclude that abundance determinations are probably affected by large temperature fluctuations in the gas, caused by additional heating mechanisms such as shocks by high speed ejecta and photo-electrons from dust grains, etc. Our kinematical analysis clearly demonstrates that H lines are not emitted in the inner knots but in the outer shell. In the outer zone we have detected a high-velocity compact structure, with velocities from −40 to 90 km s^{-1}. This *spike* emits in collisionally excited lines (mainly [O III]), but it is not detected in H or He lines. Therefore, it should consist of a "bullet" of H-deficient material that is colliding with the outer shell.

Key Words: **ISM: ABUNDANCES — ISM: KINEMATICS AND DYNAMICS — PLANETARY NEBULAE: INDIVIDUAL (ABELL 78)**

1. INTRODUCTION

Abell 78 (A 78) is a well known member of a small (only five members known) but important class of planetary nebulae (PNe) that are characterized by hydrogen-poor, dusty ejecta. In these nebulae, the H-poor material is surrounded by an outer normal H-rich envelope, indicating that a secondary ejection of highly processed material occurred after the loss of the H-rich envelope of the AGB progenitor.

[1]Based upon data collected at the Observatorio Astronómico Nacional in San Pedro Mártir, B. C., México.

It seems evident that the central stars have had a huge mass-loss phase in previous epochs (Wolf-Rayet phase). As a matter of fact, one of these objects, A 58, has presented a nova-like outburst, ejecting H-deficient C-rich material, in 1919. The central stars show, presently, helium and carbon emission lines; therefore, they have been classified as early Wolf-Rayet stars of the carbon sequence ([WCE]), although, due to the weakness of the stellar lines, Tylenda, Acker, & Stenholm (1993) have classified them as *weak emission line stars*.

The nucleus of A 78 presents intense P Cygni profiles in lines of highly ionized elements such as C IV λ1550, O V λ1371 and N V λ1240 (Heap 1979; Kaler & Feibelman 1984). By computing models of expanding atmospheres, Leuenhagen, Koesterke, & Hamman (1993) have analyzed the stellar emission-line spectrum, deriving an effective temperature of $T_\star = 1.15 \times 10^5$ K, a mass-loss rate of $\log \dot{M} = -5.2\ M_\odot\ \mathrm{yr}^{-1}$, and a chemical composition of $\beta_{\mathrm{He}} = 33$, $\beta_{\mathrm{C}} = 50$, $\beta_{\mathrm{N}} = 2$, and $\beta_{\mathrm{O}} = 15$, in percentage of mass fraction. Similar results have been reported by Werner & Koesterke (1992) from analysis of the photospheric absorption spectra. Based upon these results, Koesterke & Werner (1998) have classified the star as a transition [WC]-PG1159 type star.

Trying to unveil some of the unknowns concerning PNe with H-deficient central stars, we have started a program of systematic observations of these objects, to obtain spatially resolved spectroscopic data of the nebulae. These data are used to derive the chemical composition and to determine the kinematic properties of the ionized gas. A sample of [WCE] objects was analyzed by Peña et al. (1998). In this work, the data for A 78 is discussed.

In Figure 1 we present an [O III] λ5007 image of A 78 obtained by us. A complex morphology is evident: a faint extended and somewhat elliptical outer-shell surrounds a bright and knotty inner-shell of about 40″ by 60″. In the center, a flat structure at P.A. 135°.0 contains several bright knots, around the central star. Jacoby (1979) noticed that the faint outer envelope is much brighter in hydrogen lines than in [O III] λ5007.

A 78 is also a well known infrared emitter: Cohen & Barlow (1974), Cohen et al. (1977) and Kimeswenger, Kerber, & Weinberger (1999) have reported strong IR emission near the nucleus, suggesting thermal emission from dust in the central 10″ radius. Jacoby (1979) and Hazard et al. (1980) showed that the IR emission coincides with the inner knots which are bright at [O III] λ5007 but undetectable in the hydrogen lines. The weakness of H lines has been shown to be caused by an extreme hydrogen-deficiency (Hazard et al. 1980; Jacoby & Ford 1983; Manchado, Pottasch, & Mampaso 1988). All these authors have agreed that the H-depleted material appears to be the end product of a H-burning shell that has subsequently been ejected. Jacoby & Ford (1983) have found that the relative abundances of oxygen, nitrogen and neon are not very different from the typical values of normal planetary nebulae; while Manchado et al. (1988) have reported strong density and abundance gradients across the nebula, the gas being denser and very heavy-element enriched in the inner zones.

Several kinematic studies of A 78 have been performed, showing the large complexity of the nebula. Pişmiş (1989) indicates a heliocentric velocity of -3.0 ± 10 km s^{-1}, whereas Acker (1992) report a value of 27 km s^{-1}.

Harrington, Borkowski, & Tsvetanov (1995) obtained HST spectroscopic data of the stellar C IV λ1550 emission and found a series of blue-shifted absorptions with velocities ranging from -18 to -385 km s^{-1} superposed on the P Cygni profile, indicating the presence of a mass-loading wind in A 78. Large C^{+3} column densities are reported by these authors.

More recently, from spatially resolved profiles of the [O III] λ5007 line for several zones of A 78, Meaburn et al. (1998) report a heliocentric radial velocity of the system, $V_{\mathrm{SYS}} = -22 \pm 2$ km s^{-1} and a radial expansion velocity of 40 km s^{-1} for both, the outer H-rich and the knotty inner shell. Although, the inner shell presents a more complex kinematical structure and high velocity structures (*spikes*), starting from the blue side of the inner shell and extending an additional -140 km s^{-1} or more, have been found by these authors.

In this work, we analyze high resolution *echelle* spectrophotometric data of different regions of A 78: the central zone, the bright knots around the star, and the outer H-rich nebula, trying to determine the kinematics, physical parameters and chemical composition for each region. Observations and data reduction are described in § 2. In § 3, the kinematical analysis is presented and discussed. Physical parameters and chemical abundances are derived and discussed in § 4 and our results are presented in § 5.

2. OBSERVATIONS AND DATA REDUCTION

The observations were carried out with the 2.1 m telescope (f/7.5) at the Observatorio Astronómico Nacional in San Pedro Mártir, B. C., México on 1995 July 24–31 and 1999 October 4–7. High-resolution

spectra were obtained using the REOSC Echelle Spectrograph (Levine & Chakrabarty 1994).

In the first run, a resolution of 0.24 Å per pixel at Hα was obtained using the University College London camera and a CCD-Tek detector (1024 × 1024, 24 μm × 24 μm pixels). The wavelength coverage was 3500 Å to 6650 Å. For the second season, a 2048 × 2048, 14 μm × 14 μm pixel CCD-Tek detector was used, covering a wavelength interval from 3360 Å to 7360 Å with a wavelength accuracy of about 0.19 Å per pixel in average.

A Th-Ar lamp was observed for wavelength calibration and a tungsten bulb was used for flat fielding. Standard stars from the list by Hamuy et al. (1992) were observed each night for flux calibration.

The three regions of A 78 observed are marked in Figure 1. Region 1 corresponds to the central zone including the central star. For Region 2, the slit was centered in the star and oriented along the flat structure with P.A. 135°.0 including the bright knots present there. Region 3 is located as 35″ from the star, and sections of both, the outer H-rich shell and the knotty inner shell, were included in the slit. For all the observations, the slit length was large enough to allow for a spatially resolved spectral analysis. The log of observations are listed in Table 1.

Data reduction was performed using the package IRAF[2] and includes standard bias-subtraction and flat-field correction for all spectra. In order to increase the S/N ratio, the spectra at the same position were averaged. To determine the line fluxes, the spectra were extracted including all the detected emission along the slit and were wavelength and flux calibrated. Some examples of the flux calibrated *echelle* extracted orders are presented in Figure 2. For the kinematical analysis, some sections of the 2D spectra were wavelength calibrated (see Figures 3 and 4).

3. KINEMATICAL ANALYSIS

A careful search for nebular lines in the spectra of each region was performed. The lines detected are presented in Table 2. Some of them show complex profiles with several components. Our high-resolution spectra allowed us to perform a detailed analysis of such components, which is presented in this section.

For the kinematical analysis, we have adopted a systemic heliocentric radial velocity, $V_{SYS} = -22 \pm 2$ km s^{-1}, as given by Meaburn et al. (1998). This value agrees with the line profiles presented here, specially with the centers of the shell-type features found.

3.1. *Regions 1 and 2: The Inner Hydrogen-Deficient Knots*

Regions 1 and 2 correspond to the central zones around the star. The gas present there is the nearest to the stellar nucleus and it is probably the most affected by the intense UV radiation and the mechanical energy of the stellar wind. The Region 1 13″ length slit, oriented N-S, has intersected the central part of Region 2, showing the same inner knots and the same kinematical behavior. Thus, only results for Region 2 will be presented.

We made special efforts to include in the 20″ slit all the flat structure along P.A. 135°.0. The HST archive image U2QY010CT shows that it consists of several filaments and knots. Several heavy-element and some helium nebular lines were found, but no hydrogen lines, except Hα were detected in this position.

In Figures 3*a* and 3*b*, position-velocity contour diagrams of [O III] λ5007 and Hα for Region 2 are presented. Only the emission detected three-sigma above the noise level is shown. The stellar continuum is very intense and can be used as a reference frame. From these figures, it is evident that the two lines show complex, but very different, velocity structures.

The Hα emission shows a faint and knotty shell-like structure, more or less centered at the system velocity, with a difference $\Delta V \sim 80$ km s^{-1}, between the red and blue components (this corresponds to twice the expansion velocity of the shell). At both sides of the central star, the blue component is much fainter than the red one. This is specially noticeable in the upper part of the diagram (NW direction), where the blue component is almost undetectable. The faint emission at 6558 Å corresponds to He II. This emission shows a velocity structure more similar to that of [O III] λ5007 than to Hα.

The [O III] λ5007 contours (Figure 2*a*) are very different from Hα ones. They do not correspond to an expanding shell or disk, but to a knotty bipolar structure. Two well resolved knots near the central star, have been detected (marked **a** and **b** in Figure 2*a*). They are blue-shifted relative to V_{SYS}, showing velocities of -59 ± 30 km s^{-1} and -17 ± 40 km s^{-1} (both uncertainties correspond to the FWHM), respectively. Knot **b** is the nearest to the central star, at about 2″ projected distance, and seems to have a complex structure, not resolved in our spectrum. Knot **a** extends towards the SE in a faint cometary tail with a velocity bluer than the

[2]IRAF is distributed by NOAO, which is operated by AURA, Inc. under contract with the NSF.

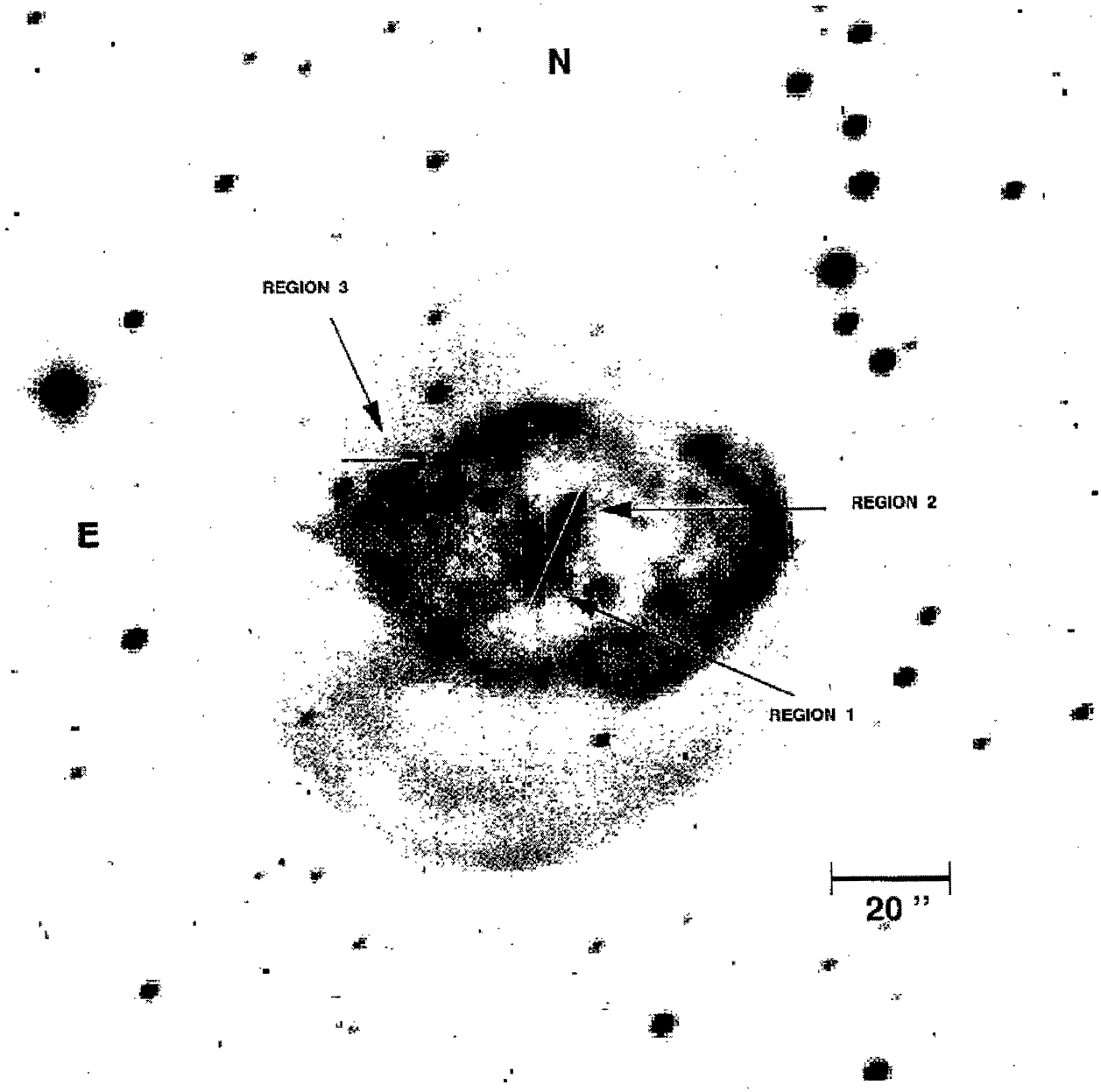

Fig. 1. [O III] λ5007 image of A 78 (15 min exposure time) obtained with the 2.1 m telescope at OAN in San Pedro Mártir, México on 1995 July 27. The three analyzed regions are indicated by lines showing the slit orientation.

TABLE 1

OBSERVING LOG

Region	Observing date (d/m/y)	Detector	Wavelength range (Å)	Exposure time (seconds)	Slit size ($''^2$)	P.A. (°)
1	30/07/95	CCD-Tek	3500–6650	900	8×13	0
	30/07/95	CCD-Tek	3500–6650	900	2×13	0
2	31/07/95	CCD-Tek	3500–6650	900	2×13	135
	31/07/95	CCD-Tek	3500–6650	900	4×20	135
3	4/10/99	CCD-2K	3360–7360	900	4×13	90
	4/10/99	CCD-2K	3360–7360	900	8×13	90

main body of the knot. The region marked with **c** presents a velocity split centered at V_{SYS}, with a difference $\Delta V \sim 84$ km s^{-1} from peak to peak.

Considering their differences in velocity structure, it is evident that Hα and [O III] emissions come from different zones of the nebula: λ5007 is emitted preferentially in the inner knots showing a velocity structure similar to a jet-like ejection. Hα comes from portions of the outer H-rich shell intersected by the slit. This outer shell is expanding at a velocity of about 40 km s^{-1}. Other emission lines such as He II λ4686, [N II] λ6583 and [Ne III] λ3869, although very faint, seem to present velocity structures similar to [O III] λ5007, providing evidence that they come mainly from the inner knots.

3.2. *Region 3: The Outer Hydrogen-Rich Nebula*

Spectra of this zone, located at 35″ to the northeast of the central star, show a highly ionized gas. No low ionization lines are detected (see Table 2). The strongest nebular lines are [O III] $\lambda\lambda$4959 and 5007 but several hydrogen lines, as well as He II λ4686 and [Ne III] λ3869 were also detected.

Figures 4*a* and 4*b* present position-velocity contour diagrams of [O III] λ5007 and Hα for this region. In this case, the slit was oriented E-W. Similar to Region 2, here the velocity structures of the hydrogen and [O III] lines are also different.

The [O III] λ5007 diagram shows two well defined components: one is a spatially-extended narrow emission centered at the system velocity, which seems to be part of the outer expanding shell. The other component is a bright unresolved (less than 1″) structure which shows an almost homogeneous surface brightness and extends in velocity range from -90 km s^{-1} to 40 km s^{-1}, relative the V_{SYS}. This velocity structure, stretching out for about 130 km s^{-1}, is very similar to the *velocity spikes* described by Meaburn et al. (1998).

In Figure 4*b*, it is evident that there is not such a high-velocity structure in the Hα emission. Hydrogen emission is spatially extended, with a velocity structure similar to the extended [O III] emission. It is worth to emphasize that neither the He II λ4686 emission line (not shown here) does present the *spike*. In the case of the faint [Ne III] λ3869 emission, the high-velocity structure is barely detected.

3.3. *Discussion*

The compact high-velocity structure found in Region 3, emits in [O III] λ5007 and other heavy-element collisionally excited lines but it is not detected in H or He lines. The lack of H-emission in *spikes* can be understood if the gas in the high-velocity structure is H-deficient, similar to that in the inner knots. The absence of He lines in the *spike* is, however, harder to explain considering that the H-deficient material is He-rich. A possible explanation emerges if we assume that the emission from *spikes* is mainly produced by shocks. A few shock models of photoionized gas have been published in the literature and they usually predict much fainter emission of He II than [O III] lines. For instance, for a shock at 100 km s^{-1} against an ionized gas, Cox & Raymond (1985) computations predict $I(\lambda4686)/I(\lambda5007) \leq 0.02$. If this is the case, our sensitivity would not allow us to detect He II emission.

Remarkably, no *spike* has been detected in the central knots (Regions 1 and 2). Such high-velocity structures appear at 20″ or 30″ away from the central star, associated to the inner knotty shell.

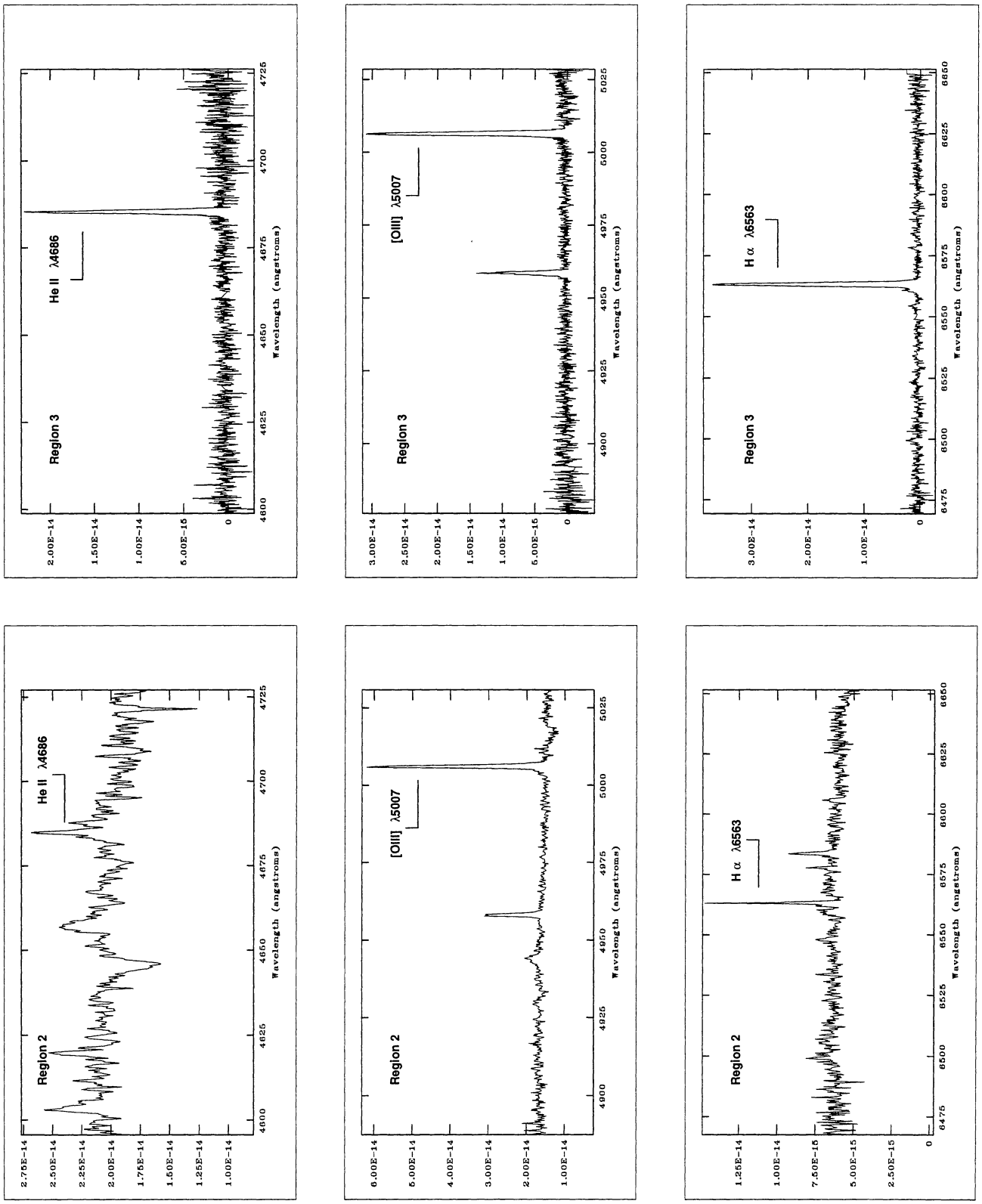

Fig. 2. Flux calibrated *echelle* orders are shown for Region 2 (central knots including the central star) and Region 3 (outer envelope). The spectrum of Region 2 showing He II λ4686 is smoothed with a box size of 3.

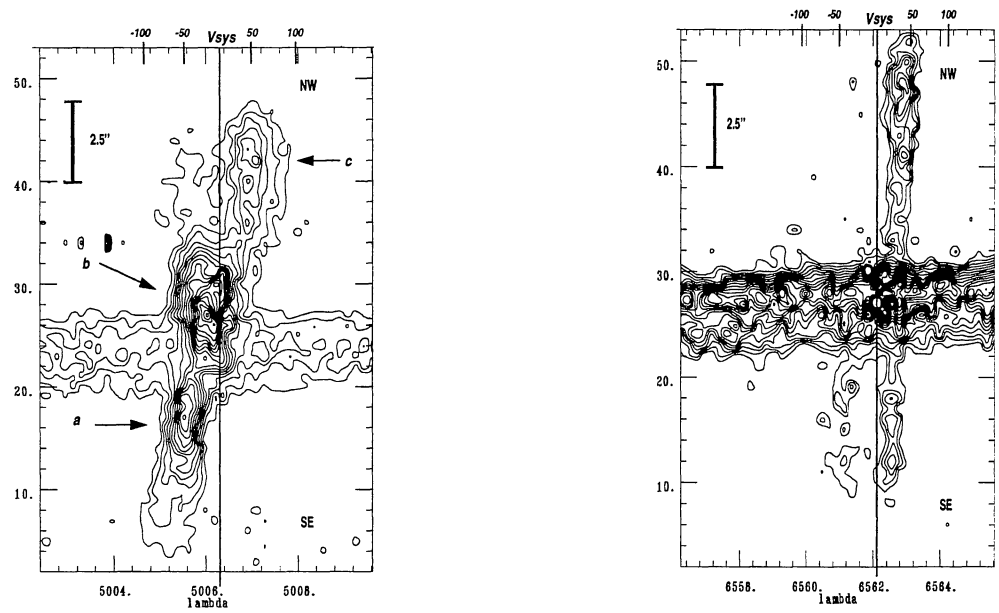

Fig. 3. For Region 2, the position-velocity contour diagram of *a*) [O III] λ5007 and *b*) Hα are presented. The systemic velocity is indicated by a vertical line and the upper scale is in km s^{-1}. The spots in the center of Hα emission are due to defectuously removed cosmic rays.

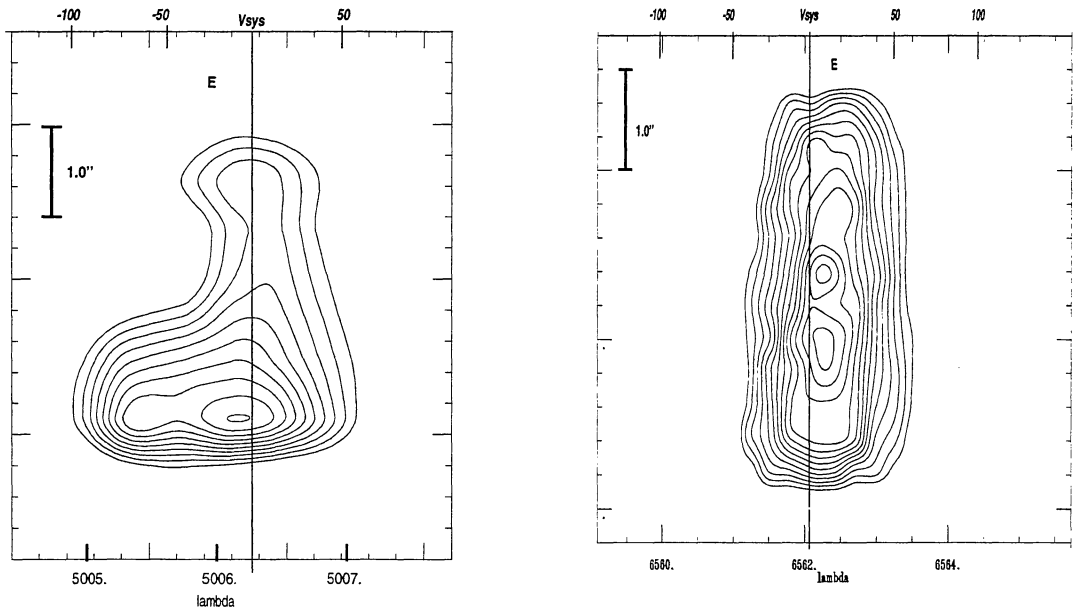

Fig. 4. For Region 3, we present position-velocity contour diagrams of *a*) [O III] λ5007 and *b*) Hα . The systemic velocity is indicated by a vertical line and the upper scale is in km s^{-1}.

TABLE 2

DEREDDENED NEBULAR INTENSITY LINE RATIOS RELATIVE TO $I(\lambda5007) = 100$

λ_{lab} (Å)	Ion	$f(\lambda)$[a]	$I(\lambda)$[b]		
			Region 1	Region 2	Region 3
3726.0	[O II]	0.266	4.4:	6.0:	< 6.4
3728.8	[O II]	0.265	4.1:	5.4:	...
3868.7	[Ne III]	0.228	11.5	13.5	11.3
4101.8	Hδ	0.172	...	...	7.8
4340.5	Hγ	0.129	...	...	14.0
4363.2	[O III]	0.124	3.5:	3.0	3.8
4685.7	He II	0.042	17.0	21.5:	27.0
4711.3	[Ar IV]	0.036	...	...	2.6
4714.1	[Ne IV]	0.035	5.9:	4.6:	< 1.0
4725.0	[Ne IV]	0.033	5.8:	4.2:	< 1.9
4740.2	[Ar IV]	0.029	...	...	1.8
4861.3	Hβ	0.000	...	...	29.9
4958.9	[O III]	−0.023	35.3	34.6	32.6
5006.8	[O III]	−0.034	100.0	100.0	100.0
5875.7	He I	−0.216	2.1	1.6	< 1.5
6548.0	[N II]	−0.321	1.1	1.8	...
6562.8	Hα	−0.323	6.7	7.6	57.8
6583.4	[N II]	−0.326	4.4	4.8	...
$F(\lambda5007)$ (10^{-13} erg cm^{-2} s^{-1})			2.27	0.60	1.36

[a] Reddening law from Seaton (1979).

[b] A reddening correction $c(H\beta) = 0.40$ was used for all positions.

They probably correspond, as suggested by Meaburn et al. (1998), to high-velocity 'bullets', such as those reported by Clegg et al. (1993), colliding with the outer shell.

The kinematics of the knots in the central zone shows that the flat structure containing them is not a radially expanding disk. At least three components at different velocities, designated **a, b** and **c** in our Fig. 2, have been found. Knot **a**, located a few arcseconds SE of the central star with $V \sim -50$ km s^{-1}, relative to V_{SYS}, extends in a faint blue-shifted cometary tail opposite to the central star. The tail is probably due to material ablated and accelerated by the hyper-sonic stellar wind.

Knot **b** projects nearest the central star. It has a mean radial velocity close to V_{SYS}, but it shows a complex structure not well resolved with several emission peaks whose velocities range ±40 km s^{-1} relative to the mean value. As with knot **a**, knot **b** seems to be strongly affected by the UV radiation and the fast wind from the star. The hard environmental conditions for the central knots have been studied by Borkowski et al. (1993) who concluded that additional heating by photo-electrons from dust grains is important in these knots.

4. PHYSICAL PARAMETERS AND CHEMICAL COMPOSITION

One-dimensional spectra of the different observed regions were obtained by extracting all the nebular

TABLE 3

PHYSICAL PARAMETERS AND IONIC ABUNDANCES RELATIVE TO H^+

Ion[a]	$\cdots\lambda$(Å)	Region 1	Region 2	Region 3
He^+	$\cdots$5876	0.54 ± 0.32	0.38 ± 0.27	< 0.03
He^{+2}	$\cdots$4686	0.72 ± 0.36	0.79 ± 0.40	0.09 ± 0.04
N^+	$\cdots$6584	0.08 ± 0.04	0.09 ± 0.04	...
O^+	$\cdots$3727	0.14 ± 0.07	0.22 ± 0.10	0.008 ± 0.005
O^{+2}	$\cdots$5007	2.16 ± 0.70	2.30 ± 0.70	0.16 ± 0.05
Ne^{+2}	$\cdots$3869	0.52 ± 0.25	0.67 ± 0.36	0.04 ± 0.02
Ne^{+3}	$\cdots$4725	3.17 ± 1.60	6.32 ± 3.16	0.14 ± 0.08
Ar^{+3}	$\cdots$4711	...	...	0.002 ± 0.01
T_e([O III]) (10^4 K)		2.07 ± 0.10	1.88 ± 0.10	2.15 ± 0.20
N_e([O II]) (10^2 cm^{-3})		7.3 ± 2.2	7.9 ± 2.6	–
N_e([Ar IV]) (10^2 cm^{-3})		...	...	$< 1\ ^{+0.30}_{-0.07}$

[a] Except for helium, all values are in units of 10^{-4}.

emission for each detected line, and calibrating the resulting fluxes.

The spectrum of Regions 1 and 2 are dominated by the stellar continuum and broad stellar emission lines such as C IV $\lambda\lambda$5800, 5812 and N V $\lambda\lambda$4603, 4620. Several nebular lines are also present, [O III] $\lambda\lambda$4959, 5007 being the brighter ones. These lines are emitted mainly in the bright knots **a** and **b** of Fig. 3*a*. He II λ4686, He I λ5876 and other heavy-element lines are also detected. Hα is the only detectable hydrogen line and, as discussed in § 3, it comes from the external shell. The nebular emission detected from Region 2 (inner knots) is fainter due to the smaller slit width (see Table 1).

Region 3 (outer shell) presents a highly-ionized nebular spectrum. The strongest lines are [O III] $\lambda\lambda$4959, 5007 and He II λ4686. He I λ5876 and the low ionization lines are extremely faint or absent. Several hydrogen lines were detected. This allowed us to measure the extinction towards A 78. A logarithmic reddening coefficient $c(H\beta)$ of 0.40 ± 0.15 was obtained from the Hβ , Hγ and Hδ intensity ratios assuming case B recombination theory (Hummer & Storey 1987). Our value is about 0.2 dex larger than values reported previously (Cohen et al. 1977; Manchado et al. 1988). We have assumed that the value for Region 3 is representative of the whole nebula.

To deredden the observed line fluxes, Seaton (1979) extinction law was used. Adopted values for the Seaton's law, $f(\lambda)$, and dereddened intensities for the three observed regions, relative to [O III] λ5007, are listed in Table 2. For all regions, errors in the flux measurements are correlated with the line intensity. Line fluxes brighter than 5×10^{-14} erg cm^{-2} s^{-1} have uncertainties of 10%. Line fluxes between 1 and 5×10^{-14} erg cm^{-2} s^{-1} are accurate within a factor of 1.5. Line fluxes below 1×10^{-14} erg cm^{-2} s^{-1} have larger uncertainties (a factor of 1.7).

4.1. *Physical Parameters*

Despite the faintness of the nebular material, the high spectral resolution and the wide wavelength range observed has allowed us to perform a plasma diagnosis. Electron temperatures were derived from [O III] $I(\lambda4363)/I(\lambda5007)$ ratios and electron densities were estimated from the [O II] $I(\lambda3726)/I(\lambda3729)$ and [Ar IV] $I(\lambda4740)/I(\lambda4711)$ ratios, when available. The results are listed in Table 3. Plasma diagnosis and ionic abundances were computed using the routine ABELION, kindly provided by G. Stasińska (this routine computes line emissivities at different T_e and N_e using the atomic parameters given in Stasińska & Leitherer 1996).

Our electron temperatures are near 20,000 K for all the regions which is a very high value for a photoionized gas. Comparing our results with previous determinations, we found that the average of electron temperatures for Regions 1 and 2 is similar, within uncertainties, to the 17,500 K found by Man-

chado et al. (1988) for their region 4, which partially coincides with our central zones. On the other hand, from the [O II] density sensitive ratio, we derived an electron density about 2 times lower than the *rms* value estimated by Manchado et al. (1988) for the same region.

For the outer shell (our Region 3), our T_e of 21,000 K is similar to the value of 19,000 K derived by Manchado et al. (1988) for their region 1 nearby, and our upper limit of 100 cm^{-3} for the electron density from the [Ar IV] density sensitive line ratio, is also in agreement with their *rms* density. We have no evidence of the low temperature zones, with $T_e \sim$ 13,000 K, reported by Jacoby & Ford (1983).

4.2. *Chemical Composition*

4.2.1. *Ionic Abundances*

Ionic abundances of He^+, He^{+2}, N^+, O^+, O^{+2}, Ne^{+2}, Ne^{+3}, and Ar^{+3}, relative to H^+, were derived from the line intensities given in Table 2 and the physical parameters of Table 3. Uncertainties in abundances depend upon the strength of the lines and the uncertainties in the physical conditions (T_e and N_e). Abundances and uncertainties are listed in Table 3.

It should be noticed that the derived ionic abundances represent an average of the abundances integrated along the line of sight, therefore, for Regions 1 and 2, where the helium, oxygen and other heavy-element lines are emitted mainly in the inner knots, while the H emission comes from the outer shell, these averages, relative to H^+, are only lower limits to the true ionic abundances of the inner zones.

It is also important to notice that the outer shell has an extremely high ionization level and no low ionization species (O^+, N^+) are detected. Even He I λ5876 emission line is almost undetectable in this zone. This is not the case for the spectrum of the inner knots, where the low ionization species are clearly seen and their ionic abundances can be computed.

4.2.2. *Total Abundances*

From the ionic abundances, total abundances were derived. He/H abundance ratios were computed by assuming that

$$He/H = (He^+ + He^{+2})/H^+. \quad (1)$$

For oxygen, we present two estimates. The first was derived using the ionization correction factors (*ICF*s) proposed by Kingsburgh & Barlow (1994) to correct for the unseen ions (mainly O^{+3} and O^{+4}), that is

$$O/H = (O^+ + O^{+2})/H^+ \times [(He^+ + He^{+2})/He^+]^{2/3}. \quad (2)$$

TABLE 4

ABUNDANCES BY NUMBER

Ratio	Region 1	Region 2	Region 3	⟨ PN ⟩[a]
He/H	1.26	1.17	< 0.12	< 0.12
O/H[b]	4.03	5.30	> 0.42	4.79
O/H[c]	15.2	23.8	0.77	
N/O	0.60	0.23	...	0.47
Ne/O	0.24	0.29	0.24	0.26
Ar/O	...	...	0.01	0.004

[a] Taken from Kingsburgh & Barlow (1994).
[b] O/H ratios (in units of 10^{-4}) from Kingsburgh & Barlow (1994) *ICF*.
[c] O/H ratios (in units of 10^{-4}) from $O^{+2}/H^+ \times (Ne^{+2} + Ne^{+3})/Ne^{+2}$.

The results are presented in the second line of Table 4. It is well known that *ICF*s for O, based upon the helium ionization structure, break down for very highly ionized nebulae (Kingsburgh & Barlow 1994) which is the case of A 78, therefore we have computed another O/H ratio, by assuming that

$$O/H = O^{+2}/H^+ \times (Ne^{+2} + Ne^{+3})/Ne^{+2}. \quad (3)$$

That is, we have assumed that the Ne/O abundance ratio is constant and equal to Ne^{+2}/O^{+2}, and we have used the Ne^{+3} abundance (although very uncertain) to correct for the unseen presence of O^{+3}. In this case we are not correcting for the presence of O^{+4}, but it is probably much less abundant than O^{+3}. The latter O/H ratios, presented in line 3 of Table 4, are much larger, for the three observed regions, than those based on He *ICF*s. We consider that these higher O/H determinations are more reliable but, as discussed in § 4.3, they are probably only lower limits to the true O/H ratios.

For nitrogen, neon, and argon, the total abundances were estimated relative to oxygen, according to the following rules, which were taken from the *ICF* squeme proposed by Kingsburgh & Barlow (1994):

$$N/O = N^+/O^+, \quad (4)$$

$$Ne/O = Ne^{+2}/O^{+2}, \quad (5)$$

$$Ar/O = Ar^{+3}/O^{+2}. \quad (6)$$

The results are listed in Table 4, and compared with the average values found for Galactic planetary nebulae (Kingsburgh & Barlow 1994).

4.3. *Discussion*

Our data come from two very well differentiated zones of the nebula: the inner knots and the outer H-rich shell. Estimates of chemical abundances were made assuming that photoionization is the only exciting mechanism and thus, the electron temperatures presented in Table 3 are representative of the whole nebula. The possibility of having large temperature fluctuations in the gas is discussed below.

Independently of temperature fluctuation effects, it is evident that the core knots show a extreme hydrogen deficiency. Total abundances of helium, oxygen and other heavy elements relative to H, derived for this zone, are only lower limits if we consider that the kinematical differences between the H and heavy-element emissions along this sight-line show that H lines are emitted in the outer zone. Therefore, we conclude that there is virtually no hydrogen in the central knots. The chemical composition is dominated by helium and, probably, carbon (large column densities of C^{+3} have been derived for the central zones by Harrington et al. 1995, which unfortunately are not observable in the optical). Due to the absence of hydrogen, O, Ne, and N seem to be very enriched, but the relative abundances Ne/O and N/O, derived from the Ne^{+2}/O^{+2} and N^{+}/O^{+} ratios, are equal, within uncertainties, in all the studied zones and similar to the averages for disk PNe.

A rough estimate of the present O abundance relative to the initial H (O_{pres}/H_{init}) can be made if a complete conversion of H into He is adopted. Taking into account an initial He/H $\sim$ 0.1, and considering no conversion of He into C, we have

$$He_{pres} = 0.25\ H_{init} + 0.1\ H_{init},$$

therefore,

$$O_{pres}/H_{init} = 0.35\ (O_{pres}/He_{pres}).$$

From the values of the third line in Table 4, an average $O_{pres}/H_{init} \sim 5.7\times 10^{-4}$ is found for Regions 1 and 2, which is similar to the O/H ratio of normal disk PNe. Thus we conclude that there is no heavy-elements enrichment in the inner knots; only an extreme H-deficiency.

Large O, N and Ne-enrichment in the central knots have been suggested by Manchado et al. (1988) (who have used a similar squeme to derive chemical abundances). Our O_{pres}/H_{init} value is lower than their, by a factor of about 10. This is due to the huge and unrealistic Ne^{+3} ionic abundance derived by Manchado et al. (1988) for the central region, which is more than 200 times larger than Ne^{+2} abundance of the same zone.

The peculiar chemical composition of the central knots indicates that the gas there comes from zones of the star where nucleosynthesis took place before being ejected to the interstellar medium. The O abundance in the knots is not as large as predicted by the model atmosphere computed by Leuenhagen et al. (1993) for A 78 central star (He/O = 8.8, by number, for the stellar atmosphere against our ratio of about 600 for the inner knots). This may imply that the present O in the stellar atmosphere was produced after the knot ejection.

For the outer shell we have derived a remarkable low O/H value (considering any of both methods employed), compared with the average for PNe in the Galactic disk (column 5 of Table 4). Although large uncertainties in our determination make the O/H value very uncertain, we estimate that our value based upon Ne *ICF*s should be correct within a factor of three (in the extreme case where O^{+4} were three times larger than O^{+3}). An O/H ratio three times larger than the value presented in the third line of Table 4 is still very low. This apparent low metallicity in A 78 outer envelope is evidently caused by the large [O III] electron temperature found and used to derive ionic abundances and one must investigate if the photoionization-only hypothesis is correct.

Disk PNe, with stars as hot as A 78 nucleus, are much colder due to the efficient action of a large amount of cooling elements. Considering its location in the Galaxy and its heliocentric velocity, A 78 is definitely a disk object and it should have normal disk PN abundances. Therefore the high T_e, derived from the [O III] 4363/5007 line ratio, should be a consequence of additional heating mechanisms of the photoionized gas. These mechanisms could be photo-electrons from dust grains (as proposed by Borkowski et al. 1993) or/and mechanical energy deposition due to the stellar activity (high-speed shocks caused by the stellar wind, high-speed bullets, etc.). For our Region 3 we have found evidence of such mechanical energy deposition in the form of the *spike* present there. Therefore, the ionized gas should be certainly affected by strong temperature fluctuations.

The presence of T_e fluctuations in nebulae was first suggested by Peimbert (1967) and, since then, it has been studied by many authors. The net effect of including such fluctuations in ionic abundance determinations is to increase the abundances derived from

collisionally excited lines relative to abundances from H recombination lines. That means, in our case, that the O/H values presented in Tables 3 and 4 derived from T_e (O III) should be considered only lower limits to the true abundances. True abundances could be calculated only by computing an appropriate ionization structure model which, including different heating mechanisms, reproduces the relative line intensities and physical conditions in A 78. Such a model is out the scope of this work.

On the other hand, the neon and nitrogen abundance ratios relative to oxygen, derived from the Ne^{+2}/O^{+2} and N^{+}/O^{+} ionic ratios, are much less dependent on temperature fluctuations, thus they have much lower uncertainties. Our values for Ne/O and N/O abundance ratios are normal. Therefore, the heavy element abundances in the external hydrogen-rich nebular zones of A 78 seems to be similar to the average values found in normal disk planetary nebulae.

5. RESULTS

From our kinematical analysis, we confirm that the external H-rich envelope has an expansion velocity of about 40 km s^{-1}, in agreement with the analysis of Meaburn et al. (1998) and Manchado et al. (1988). The two components of the outer shell are reasonably centered around a systemic velocity $V_{SYS} \sim -22$ km s^{-1}, consistent with the value reported by Meaburn et al. (1998) and in contradiction with the 27 km s^{-1} from Acker et al. (1992).

By comparing the kinematical behavior of Hα and [O III] λ5007 emission lines in different zones of A 78, we have demonstrated that no H lines are emitted in the inner knots. These knots, distributed in a flat structure around the central star, are composed of extreme H-deficient ejecta arising from zones of the star were H- and probably He-burning took place. The knots present radial velocities of about $\pm$ 50 km s^{-1}, relative to V_{SYS} and show cometary tails at higher velocities, suggesting that material is being ablated by the stellar wind.

A high-velocity structure (similar to the [O III] λ5007 *spikes* reported by Meaburn et al. 1998) has been found in the outer knotty shell, extending in a velocity range from -40 to 90 km s^{-1}. Our *spike* is detected only in collisionally excited lines of heavy elements, showing no emission in H nor He lines. Therefore we conclude that *spikes* should be H-deficient 'bullets' ejected by the star, which are colliding with the external nebular shell. The absence of He II lines in the *spike* is probably due to the shock conditions exciting the *spike* emission.

Physical parameters derived from our spectrophotometric data show that the ionized gas has a very high electron temperature of about 20,000 K in all the studied zones, while the electron density varies from 700 cm^{-3} in the inner knots to less than 100 cm^{-3} in the outer shell. With these physical parameters, we have derived the O, N, and Ne abundances in the different zones of the nebula finding that the inner knots are extremely H-deficient, but not O-, N- or Ne-enriched.

A remarkable low O/H ratio is found for the outer shell (six times lower than the average value in disk PNe). We conclude that abundance determinations in A 78 are strongly affected by temperature fluctuations caused by different heating mechanisms (photoionization, shocks, photo-electrons from dust grains, etc.) and represent only lower limits to the true abundances of the nebular gas. On the other hand, Ne/O and N/O abundance ratios are less affected by such temperature fluctuations and the values obtained are confident and normal in all the explored zones.

Due to its interesting and complex kinematics produced by strong interaction between the original nebula and the present highly processed stellar ejecta, A 78 is an excellent object to study mass-loaded flows and the evolution of intermediate mass stars that suffer high mass loss events in advanced evolutionary stages. In this sense, a great effort should be made to determine the important carbon abundance in the inner knots in order to analyze the stellar nucleosynthesis processes.

The authors are grateful to G. Stasińska for supplying the ABELION program, which was used to calculate the physical parameters and the ionic abundances from the data. Invaluable comments by M. Richer, M. Peimbert, and S. Torres-Peimbert are deeply appreciated. This work was partially supported by DGAPA/UNAM (grants IN-109696 and IN-100799). S.M. acknowledges scholarship by DGEP/UNAM.

REFERENCES

Acker, A., Ochsenbein, F., Stenholm, B., Tylenda, R., Marcout, J., & Schohn, C. 1992, Strasbourg-ESO Catalogue of Galactic Planetary Nebulae (Garching bei München: ESO)

Borkowski, K. J., Harrington, J. P., Tsvetanov, Z., & Clegg, R. E. S. 1993, ApJ, 415, L47

Clegg, R. E. S., Devaney, M. N., Doel, A. P., Dunlop, C. N., Major, J. V., Myers, R. M., & Sharpless, R. M. 1993, in IAU Symp. 155, Planetary Nebulae,

eds. R. Weinberger & A. Acker (Dordrecht: Kluwer), 388
Cohen, M., & Barlow, M. J. 1974, ApJ 193, 401
Cohen, M., Hudson, H. S., O'Dell, S. L., & Stein, W. A. 1977, MNRAS 181, 233
Cox, D. P., & Raymond, J. C. 1985, ApJ 298, 651
Hamuy, M., Walker, A. R., Suntzeff, N. B., Gigoux, P., Heathcote, S. R., & Phillips, M. M. 1992, PASP, 104, 533
Harrington, J. P., Borkowski, K. J., & Tsvetanov, Z. 1995, ApJ, 439, 264
Hazard, C., Terlevich, R., Morton, D. C., Sargent, W. L. W., & Ferland, G. 1980, Nat., 285, 463
Heap, S. R., 1979, in IAU Symp. 83, Mass Loss and Evolution of O-Type Stars, eds. P. S. Conti & C. W. H. de Loore (Dordrecht: Reidel), 99
Hummer, D. G., & Storey, P. J. 1987, MNRAS, 224, 801
Jacoby, G. H. 1979, PASP, 91, 754
Jacoby, G. H., & Ford, H. C. 1983, ApJ, 266, 298
Kaler, J. B., & Feibelman, W. A. 1984, ApJ, 282, 719
Kimeswenger, S., Kerber, F., & Weinberger, R. 1999, MNRAS, 296, 614
Kingsburgh, R. L., & Barlow, M. J. 1994, MNRAS, 271, 257
Koesterke, L., & Werner, K., 1998, ApJ, 500, L55
Leuenhagen, U., Koesterke, L., & Hamann, W.-R. 1993, Acta Astr., 43, 329
Levine, S., & Chakrabarty, D., 1994, Reporte Técnico No. MU-94-04, Instituto de Astronomía (UNAM)
Manchado, A., Pottasch, S. R., & Mampaso, A. 1988, A&A, 191, 128
Meaburn, J., López, J. A., Bryce, M., Redman, M. P. 1998, A&A, 334, 670
Peimbert, M. 1967, ApJ, 150, 825
Peña, M., Stasińska, G., Esteban, C., Koesterke, L., Medina, S., & Kingsburgh, R. 1998, A&A, 337, 866
Pişmiş, P. 1989, MNRAS, 237, 611
Seaton, M. J. 1979, MNRAS, 187, 73
Stasińska, G., & Leitherer, C. 1996, ApJS, 107, 661
Tylenda, R., Acker, A., & Stenholm, B. 1993, A&A, 102, 595
Werner, K., & Koesterke, L. 1992, in Atmospheres of Early-Type Stars, eds. U. Herber & C. S. Jefferey Lecture Notes in Physics 401 (Berlin: Springer), 288

Selene Medina and Miriam Peña: Instituto de Astronomía, UNAM, Apartado Postal 70-264, 04510 México, D. F., México (selene,miriam@astroscu.unam.mx).